Available online at www.sciencedirect.com
SCIENCE DIRECT®
Journal of Solid State Chemistry 177 (2004) 1672–1680
JOURNAL OF SOLID STATE CHEMISTRY
http://elsevier.com/locate/jssc

Syntheses and structural trends of the $In_xMo_{15}S_{19}$ ($0 \leqslant x \leqslant 3.7$) compounds containing Mo_6 and Mo_9 clusters

Diala Salloum,[a] Régis Gautier,[b] Patrick Gougeon,[a,*] and Michel Potel[a]

[a] *Laboratoire de Chimie du Solide et Inorganique Moléculaire, UMR CNRS 6511, Université de Rennes 1, Institut de Chimie de Rennes, Avenue du Général Leclerc, Rennes cedex 35042, France*

[b] *Laboratoire de Chimie du Solide et Inorganique Moléculaire, UMR CNRS 6511, Ecole Nationale Supérieure de Chimie de Rennes, Institut de Chimie de Rennes, Campus de Beaulieu, Rennes cedex 35700, France*

Received 16 September 2003; received in revised form 15 December 2003; accepted 18 December 2003

Abstract

The $In_xMo_{15}S_{19}$ ($x = 0.0$, 0.10, 0.20, 0.36, 0.50, 0.70, 1.2 and 2.9) compounds were obtained from oxidation of the solid-state compound $In_{3.7}Mo_{15}S_{19}$ by iodine in sealed glass tube at temperatures below 300°C. Their crystal structures were solved and refined from X-ray single crystal data in the hexagonal space group $P6_3/m$. The Mo–S framework of the $In_xMo_{15}S_{19}$ compounds consists of an equal mixture of $Mo_6S_8S_6$ and $Mo_9S_{11}S_6$ cluster units interconnected through Mo–S bonds. The X-ray single-crystal study of the $In_xMo_{15}S_{19}$ ($0 \leqslant x \leqslant 3.7$) compounds has allowed us to follow the evolution of the Mo–Mo distances within the Mo_6 and Mo_9 clusters as a function of the cationic charge. Quantum chemical calculations carried out in order to understand these trends as well as magnetic susceptibility measurements are also reported.

Keywords: Molybdenum; Clusters; Soft chemistry; Topotactic reaction; Single-crystal; Crystal structure; Extended Hückel calculations

1. Introduction

In a recent paper, we presented the crystal structure of $In_{3.7}Mo_{15}S_{19}$ [1] which is closely related to that of the selenides $In_{2.9}Mo_{15}Se_{19}$ and $In_{3.3}Mo_{15}Se_{19}$ [2] that were the first compounds containing a transition metal cluster with a nuclearity higher than 6, namely, the bioctahedral Mo_9 cluster. In $In_{3.7}Mo_{15}S_{19}$, the latter cluster, which results from the face-sharing of two Mo_6 octahedra, coexists with the octahedral Mo_6 cluster in equal proportion. Both clusters are surrounded by S atoms to form $Mo_6S_8S_6$ and $Mo_9S_{11}S_6$ units that share some of their S atoms to create the three-dimensional Mo–S framework. The In atoms occupy three crystallographically different positions depending on their formal oxidation state of +1 or +3. In the following, we show that indium can be removed from the $In_{3.7}Mo_{15}S_{19}$ compound by oxidation with I_2 at low temperatures resulting in the $In_xMo_{15}S_{19}$ ($x = 0.0$, 0.10, 0.20, 0.36, 0.50, 0.70, 1.2 and 2.9) compounds. The single-crystal structures of the later eight compounds are presented and discussed in relation with the cationic charge transfer. Extended Hückel tight-binding (EHTB) calculations carried out on $Mo_{15}S_{19}$ allow the understanding of the evolution of Mo–Mo distances with respect to the cationic charge.

2. Experimental section

2.1. Syntheses

Starting materials used for the synthesis of $In_{3.7}Mo_{15}S_{19}$ were MoS_2, In_2S_3 and Mo, all in powder form. Before use, Mo powder was reduced under H_2 flowing gas at 1000°C during 10 h in order to eliminate any trace of oxygen. The molybdenum disulfide was prepared by the reaction of sulfur with H_2 reduced Mo in a ratio 2:1 in an evacuated (ca. 10^{-2} Pa Ar residual pressure) and flame-baked silica tube, heated at 800°C during two days. The purity of all starting reagents was checked by powder X-ray diffraction on an Inel curve sensitive position detector CPS 120. In order to avoid

*Corresponding author. Fax: +33-2-63-57-04.
E-mail address: patrick.gougeon@univ-rennes1.fr (P. Gougeon).

0022-4596/$ - see front matter © 2004 Elsevier Inc. All rights reserved.
doi:10.1016/j.jssc.2003.12.023

any contamination by oxygen and moisture, the starting reagents were mixed, ground together in a mortar and then cold-pressed in a purified argon-filled glove box. The pellet (ca. 3 g) was then loaded in a molybdenum crucible (depth: 2.5 cm; diam.: 1.5 cm), which was previously cleaned by heating at 1500°C in a high frequency furnace for 15 min under a dynamic vacuum of about 10^{-3} Pa and then sealed under a low argon pressure (300 hPa) using an arc welding system. The crucible was heated at a rate of 50°C h^{-1} up to 1120°C and held there for 48 h, then cooled at 100°C h^{-1} to 1000°C and finally cooled down to room temperature in the furnace. The resulting product was black and air-stable and was found as a pure phase on the basis of its X-ray powder diffraction diagram.

The $In_xMo_{15}S_{19}$ compounds with $x<3.7$ were obtained from oxidation of $In_{3.7}Mo_{15}S_{19}$ by iodine in silica tube at increasing temperature in the range 160–300°C according to the following reaction:

$$In_{3.7}Mo_{15}S_{19}+I_2 \text{ in excess?} \rightarrow In_xMo_{15}S_{19} + (3.7-x)InI_3$$

Our method differs from that described by Tarascon et al. [3] who used HCl gas at temperature ranging between 370°C and 550°C for removing the indium. This leads to compounds having different lattice parameters as reflected by the free-indium phase $Mo_{15}S_{19}$, the parameters of which are $a=9.1838(2)$ and $c=19.0483(5)$ Å when it is obtained by the action of I_2 at 300°C and $a=9.218(1)$ and $c=18.077(5)$ Å when synthesized under HCl gas at 550°C. The differences between the compounds obtained by the two methods result probably from the highest temperatures used by Tarascon et al. that would lead to a rearrangement of the $Mo_6S_8S_6$ and $Mo_9S_{11}S_6$ cluster units within the unit-cell. The $In_xMo_{15}S_{19}$ compounds with $x<3.7$ decompose principally into the Chevrel phase $InMo_6S_8$ and Mo_2S_3 and the binary $Mo_{15}S_{19}$ into Mo_2S_3 and Mo at temperatures above 800°C.

In Table 1, we have summarized the conditions for the syntheses of the different $In_xMo_{15}S_{19}$ phases. The stoichiometries in indium were deduced from the single-crystal X-ray structural analyses.

2.2. Single crystal X-ray studies

The X-ray diffraction data for the eight crystals investigated were collected on an Nonius Kappa CCD diffractometer using graphite-monochromated Mo$K\alpha$ radiation ($\lambda=0.71073$ Å). The COLLECT program package [4] was used to establish the angular scan conditions (φ and ω scans) used in the data collections. The different data sets were processed using EvalCCD [5] for the integration procedure. Absorption corrections were applied using the description of the crystal faces and the analytical method described by de Meulenaar and Tompa [6]. The structures were refined using JANA2000 [7]. The positions of the Mo and S atoms in $In_{3.7}Mo_{15}S_{19}$ [1] were used in the first stage of the refinements. The In positions were revealed by subsequent difference Fourier syntheses. Relevant crystallographic data are listed in Table 2, and selected bond distances are given in Table 3.

2.3. Computational procedure

Calculations have been carried out within the extended Hückel formalism [8] with the program YAeHMOP [9]. The exponents (ξ and the valence shell ionization potentials (H_{ii} in eV) were (respectively): 1.817, −13.30 for S 3p; 1.956, −8.34 for Mo 5s; 1.921, −5.24 for Mo 5p. H_{ii} values for Mo 4d were set equal to −10.50. A linear combination of two Slater-type orbitals of exponents $\zeta_1=4.542$ and $\zeta_2=1.901$ with the weighting coefficients $c_1=c_2=0.5898$ was used to represent the Mo 4d atomic orbitals. The density of states (DOS) and crystal orbital overlap populations (COOP) were obtained using a set of 18k points.

2.4. Magnetic measurements

The magnetic susceptibility was measured using a SQUID magnetometer (MPMS-XL, Quantum Design).

Table 1
Experimental conditions for the syntheses of the $In_xMo_{15}S_{19}$ compounds

	Synthesis	Time, days	a (Å)	c (Å)	V (Å^3)
$In_{3.7}Mo_{15}S_{19}$	MoS_2, In_2S_3 and Mo at 1120°C	4	9.4291(1)	18.9527(2)	1459.29(3)
$In_{2.84}Mo_{15}S_{19}$	I_2 160°C	4	9.4236(1)	18.8955(3)	1453.19(3)
$In_{1.14}Mo_{15}S_{19}$	I_2 180°C	4	9.3381(1)	18.9518(2)	1431.19(3)
$In_{0.7}Mo_{15}S_{19}$	I_2 200°C	4	9.2947(2)	18.9884(4)	1420.66(5)
$In_{0.5}Mo_{15}S_{19}$	I_2 230°C	4	9.2551(2)	19.0135(3)	1410.44(5)
$In_{0.36}Mo_{15}S_{19}$	I_2 250°C	4	9.2390(2)	19.0289(3)	1406.66(5)
$In_{0.2}Mo_{15}S_{19}$	I_2 270°C	4	9.2163(1)	19.0501(4)	1401.33(4)
$In_{0.1}Mo_{15}S_{19}$	I_2 280°C	4	9.1999(1)	19.0597(4)	1397.05(4)
$Mo_{15}S_{19}$	I_2 300°C	4	9.1838(2)	19.0483(5)	1391.33(6)

Table 2
Crystallographic and experimental data for the $In_xMo_{15}S_{19}$ compounds

Crystal data					
Chemical formula	$In_{2.9}Mo_{15}S_{19}$	$In_{1.2}Mo_{15}S_{19}$	$In_{0.7}Mo_{15}S_{19}$	$In_{0.5}Mo_{15}S_{19}$	$In_{0.36}Mo_{15}S_{19}$
Mr	2381.2	2186.0	2128.6	2105.7	2089.6
Cell setting, space group	Hexagonal, *P*63/*m*	Hexagonal, *P*63/*m*	Hexagonal, *P*63/*m*	Hexagonal, *P*63/*m*	Hexagonal, *P*63/*m*
a, *c* (Å)	9.42360 (10), 18.8955 (2)	9.33800 (10), 18.9520 (2)	9.2947 (2), 18.9884 (4)	9.2551 (2), 19.0135 (3)	9.2390 (2), 19.0289 (3)
V (Å^3)	1453.19 (3)	1431.18 (3)	1420.66 (5)	1410.44 (5)	1406.68 (5)
Z	2	2	2	2	2
Dx (Mg m^{-3})	5.440 (1)	5.071 (1)	4.975 (1)	4.956 (1)	4.932 (1)
Radiation type	Mo*K*α	Mo*K*α	Mo*K*α	Mo*K*α	Mo*K*α
No. of reflections for cell parameters	27734	68462	36202	32117	68087
θ range (°)	2.4–45.3	2.26–42.11	2.4–42.11	2.9–40.25	2.55–40.25
μ (mm^{-1})	9.83	8.65	8.31	8.21	8.12
Temperature (K)	293	293	293	293	293
Crystal form, color	Truncated octahedra, black	Truncated octahedra, black	Truncated octahedra, black	Truncated octahedra, black	Truncated octahedra, black
Crystal size (mm)	0.12 × 0.11 × 0.10	0.08 × 0.07 × 0.06	0.12 × 0.08 × 0.06	0.09 × 0.08 × 0.08	0.08 × 0.07 × 0.07
Data collection					
Diffractometer	Nonius Kappa CCD	Nonius Kappa CCD	Nonius Kappa CCD	Nonius Kappa CCD	Nonius Kappa CCD
Data collection method	φ + ω scans	φ + ω scans	φ + ω scans	φ + ω scans	φ + ω scans
Absorption correction	Analytical	Analytical	Analytical	Analytical	Analytical
T_{min}	0.4319	0.5483	0.4850	0.5555	0.5964
T_{max}	0.4937	0.6545	0.6979	0.6069	0.6732
No. of measured, independent and observed reflections	25895, 2213, 1918	22310, 2176, 1932	20560, 2160, 1501	16699, 2017, 1562	21723, 2114, 1716
Criterion for observed reflections	$I > 2\sigma(I)$	$I > 2\sigma(I)$	$I > 2\sigma(I)$	$I > 2\sigma(I)$	$I > 2\sigma(I)$
R_{int}	0.055	0.052	0.072	0.060	0.055
θ_{max} (°)	35.1	35.1	35.1	34.6	35.1
Range of *h*, *k*, *l*	$-10 \rightarrow h \rightarrow 15$ $-15 \rightarrow k \rightarrow 15$ $-29 \rightarrow l \rightarrow 30$	$-15 \rightarrow h \rightarrow 14$ $-15 \rightarrow k \rightarrow 15$ $-27 \rightarrow l \rightarrow 30$	$-15 \rightarrow h \rightarrow 15$ $-14 \rightarrow k \rightarrow 15$ $-19 \rightarrow l \rightarrow 30$	$-14 \rightarrow h \rightarrow 11$ $-14 \rightarrow k \rightarrow 14$ $-30 \rightarrow l \rightarrow 25$	$-14 \rightarrow h \rightarrow 14$ $-14 \rightarrow k \rightarrow 14$ $-20 \rightarrow l \rightarrow 30$
Refinement					
Refinement on	*F*	*F*	*F*	*F*	*F*
$R[F2 > 2\sigma(F2)]$, w$R(F2)$, *S*	0.033, 0.036, 2.29	0.029, 0.034, 2.58	0.051, 0.053, 1.57	0.043, 0.043, 1.71	0.041, 0.042, 1.92
No. of reflections	2213 reflections	2176 reflections	2160 reflections	2017 reflections	2114 reflections
No. of parameters	67	67	62	62	62
Weighting scheme	Based on measured s.u.'s w = $1/\sigma_2(F)$	Based on measured s.u.'s w = $1/\sigma_2(F)$	Based on measured s.u.'s w = $1/(\sigma_2(F) + 0.000196F2)$	Based on measured s.u.'s w = $1/(\sigma_2(F) + 0.0001F2)$	Based on measured s.u.'s w = $1/\sigma_2(F)$
$(\Delta/\sigma)_{max}$	0.001	<0.0001	<0.0001	<0.0001	<0.0001
$\Delta\rho_{max}$, $\Delta\rho_{min}$ (e Å^{-3})	2.87, –3.65	2.36, –1.55	7.23, –2.82	4.10, –2.18	3.53, –2.24
Extinction method	B–C type 1 Lorentzian isotropic (Becker and Coppens, 1974)	B–C type 1 Lorentzian isotropic (Becker and Coppens, 1974)	None	None	None
Extinction coefficient	0.093 (10)	0.038 (11)			

Table 2 (*continued*)

Crystal data			
Chemical formula	$In_{0.2}Mo_{15}S_{19}$	$In_{0.1}Mo_{15}S_{19}$	$Mo_{15}S_{19}$
Mr	2071.2	2059.7	2048.2
Cell setting, space group	Hexagonal, $P63/m$	Hexagonal, $P63/m$	Hexagonal, $P63/m$
a, *c* (Å)	9.21630 (10), 19.0501 (2)	9.19990 (10), 19.0596 (4)	9.1838 (2), 19.0483 (5)
V (Å3)	1401.33 (3)	1397.05 (4)	1391.33 (6)
Z	2	2	2
Dx ($Mg\,m^{-3}$)	4.907 (1)	4.895 (1)	4.888 (1)
Radiation type	Mo$K\alpha$	Mo$K\alpha$	Mo$K\alpha$
No. of reflections for cell parameters	96451	82750	18337
θ range (°)	2.55–42.11	2.26–42.11	2.4–42.11
μ (mm^{-1})	8.03	7.97	7.92
Temperature (K)	293	293	293
Crystal form, color	Truncated octahedra, black	Truncated octahedra, black	Truncated octahedra, black
Crystal size (mm)	$0.12 \times 0.11 \times 0.10$	$0.08 \times 0.07 \times 0.06$	$0.12 \times 0.08 \times 0.06$
Data collection			
Diffractometer	Nonius Kappa CCD	Nonius Kappa CCD	Nonius Kappa CCD
Data collection method	$\varphi + \omega$ scans	$\varphi + \omega$ scans	$\varphi + \omega$ scans
Absorption correction	Analytical	Analytical	Analytical
T_{min}	0.5978	0.5929	0.6676
T_{max}	0.6371	0.6706	0.7358
No. of measured, independent and observed reflections	23065, 2124, 1805	20219, 2049, 1722	21660, 2047, 1634
Criterion for observed reflections	$I > 2\sigma(I)$	$I > 2\sigma(I)$	$I > 2\sigma(I)$
R_{int}	0.049	0.047	0.057
θ_{max} (°)	35.1	34.6	34.6
Range of *h*, *k*, *l*	$-8 \rightarrow h \rightarrow 14$ $-14 \rightarrow k \rightarrow 14$ $-30 \rightarrow l \rightarrow 30$	$-14 \rightarrow h \rightarrow 13$ $-13 \rightarrow k \rightarrow 14$ $-26 \rightarrow l \rightarrow 30$	$-14 \rightarrow h \rightarrow 11$ $-14 \rightarrow k \rightarrow 14$ $-29 \rightarrow l \rightarrow 30$
Refinement			
Refinement on	*F*	*F*	*F*
$R[F2 > 2\sigma(F2)]$, w$R(F2)$, *S*	0.034, 0.034, 2.37	0.031, 0.032, 2.06	0.029, 0.031, 1.49
No. of reflections	2124 reflections	2049 reflections	2047 reflections
No. of parameters	63	62	56
Weighting scheme	Based on measured s.u.'s w = $1/(\sigma_2(F) + 0.000016F2)$	Based on measured s.u.'s w = $1/(\sigma_2(F) + 0.000025F2)$	Based on measured s.u.'s w = $1/(\sigma_2(F) + 0.000025F2)$
$(\Delta/\sigma)_{max}$	0.001	0.001	<0.0001
$\Delta\rho_{max}$, $\Delta\rho_{min}$ ($e\,Å^{-3}$)	3.66, −1.98	3.00, −1.93	2.52, −2.13
Extinction method	B–C type 1 Lorentzian isotropic (Becker and Coppens, 1974)	None	B–C type 1 Lorentzian isotropic (Becker and Coppens, 1974)
Extinction coefficient	0.001 (9)		0.017 (6)

Table 3
Selected interatomic distances for the $In_xMo_{15}S_{19}$ compounds

	$In_{2.9}Mo_{15}S_{19}$	$In_{1.2}Mo_{15}S_{19}$	$In_{0.7}Mo_{15}S_{19}$	$In_{0.5}Mo_{15}S_{19}$	$In_{0.36}Mo_{15}S_{19}$	$In_{0.2}Mo_{15}S_{19}$	$In_{0.1}Mo_{15}S_{19}$	$Mo_{15}S_{19}$
Mo1–Mo1 (× 2)	2.6963(5)	2.7134(5)	2.7074(10)	2.7017(9)	2.6994(7)	2.6947(5)	2.6922(5)	2.6899(5)
Mo1–Mo1 (× 2)	2.7165(5)	2.7694(3)	2.7915(6)	2.8146(5)	2.8248(4)	2.8374(5)	2.8453(5)	2.8504(5)
Mo2–Mo2 (× 2)	2.6595(4)	2.6754(4)	2.6833(7)	2.6925(7)	2.6962(6)	2.7023(4)	2.7054(4)	2.7076(4)
Mo2–Mo3	2.7187(4)	2.7435(3)	2.7496(4)	2.7521(4)	2.7539(3)	2.7553(4)	2.7560(4)	2.7556(2)
Mo2–Mo3	2.7535(5)	2.7807(4)	2.7835(7)	2.7836(6)	2.7850(5)	2.7856(5)	2.7847(5)	2.7835(4)
Mo3–Mo3 (× 2)	2.7358(6)	2.7258(6)	2.7145(9)	2.7062(8)	2.7030(7)	2.6967(5)	2.6922(5)	2.6900(5)
Mo1–Mo2	3.2574(4)	3.1813(3)	3.1525(6)	3.1257(5)	3.1144(4)	3.0993(4)	3.0893(4)	3.0780(3)
Mo1–S1	2.4384(10)	2.4266(7)	2.4324(16)	2.4337(10)	2.4362(9)	2.4386(9)	2.4407(9)	2.4389(9)
Mo1–S1	2.4447(12)	2.4387(11)	2.442(2)	2.4427(12)	2.4450(14)	2.4467(11)	2.4473(11)	2.4459(11)
Mo1–S1	2.4959(9)	2.4757(9)	2.4705(18)	2.4629(10)	2.4620(11)	2.4553(8)	2.4547(8)	2.4510(8)
Mo1–S2	2.5032(14)	2.4753(12)	2.460(2)	2.4495(13)	2.4448(14)	2.4397(12)	2.4365(11)	2.4343(11)
Mo1–S4	2.4350(15)	2.4283(9)	2.4259(15)	2.4252(12)	2.4211(10)	2.4189(12)	2.4172(11)	2.4167(11)
Mo2–S1	2.5127(11)	2.4706(9)	2.4576(19)	2.4523(11)	2.4490(11)	2.4443(9)	2.4420(9)	2.4382(9)
Mo2–S2	2.4954(8)	2.4758(8)	2.4741(15)	2.4711(8)	2.4709(9)	2.4694(7)	2.4688(7)	2.4678(7)
Mo2–S2	2.4424(11)	2.4334(11)	2.437(2)	2.4337(12)	2.4362(14)	2.4359(10)	2.4352(10)	2.4337(10)
Mo2–S3	2.6036(6)	2.6211(6)	2.6262(11)	2.6240(11)	2.6244(9)	2.6236(6)	2.6228(6)	2.6219(6)
Mo2–S5	2.4047(14)	2.4139(9)	2.4172(15)	2.4158(12)	2.4148(10)	2.4165(12)	2.4165(11)	2.4166(10)
Mo3–S2 (× 2)	2.4463(11)	2.4276(9)	2.4238(16)	2.4128(10)	2.4084(9)	2.4031(10)	2.3982(8)	2.3908(8)
Mo3–S3	2.4719(9)	2.4593(9)	2.4598(17)	2.4577(17)	2.4548(15)	2.4513(9)	2.4503(9)	2.4501(9)
Mo3–S3	2.4675(13)	2.4648(13)	2.471(3)	2.470(3)	2.472(2)	2.4745(13)	2.4748(13)	2.4773(13)
In2–S2	2.8407(14)	2.8129(12)	2.794(3)	2.774(3)	2.764(3)	2.752(4)	2.737(7)	
In2–S3	2.9378(12)	2.8930(12)	2.861(3)	2.843(4)	2.832(4)	2.814(4)	2.789(8)	
In2–S3	2.5531(18)	2.4993(18)	2.472(5)	2.454(6)	2.442(6)	2.434(7)	2.441(14)	
In2–S4 (× 3)	2.4545(15)	2.4605(10)	2.450(2)	2.438(3)	2.435(3)	2.430(4)	2.427(7)	
In1–S1	3.3576(8)	3.3671(17)						
In1–S2	3.1006(7)	3.0596(8)						
In1–S5	2.9025(19)	2.923(4)						
In2–In2 (× 2)	3.0012(17)	3.0119(17)	2.994(5)	2.983(7)	2.975(7)	2.966(9)	2.963(17)	

3. Results and discussion

3.1. Mo–S framework

A view of the crystal structure of the parent compound $In_{3.7}Mo_{15}S_{19}$ is shown in Fig. 1. In the In-deficient compounds $In_xMo_{15}S_{19}$, the Mo–S framework is similar to that of $In_{3.7}Mo_{15}S_{19}$ and thus consists of an equal mixture of $Mo_6S_8S_6$ and $Mo_9S_{11}S_6$ cluster units interconnected through Mo–S bonds (Fig. 2). The first unit can be described as an Mo_6 octahedron surrounded by 8 face-capping inner S^i (6 S1 and 2 S4) and 6 apical S^a (S2) ligands. The Mo_9 core of the second unit results from the one-dimensional trans-face sharing of 2 octahedral Mo_6 clusters. The Mo_9 cluster is surrounded by 11 S^i (6 S2, 3 S3 and 2 S5) atoms capping the faces of the bioctahedron and 6 apical S^a (S1) ligands above the ending Mo atoms. The $Mo_6S_8S_6$ and $Mo_9S_{11}S_6$ units are centered at 2*b* and 2*c* positions and have the point-group symmetry $\bar{3}$ and 3/*m*, respectively. The sulfur atoms bridge either one (S1, S2, S4 and S5) or two (S3) Mo triangular faces of the clusters. Moreover the S1 and S2 atoms are linked to a Mo atom of a neighboring cluster. The Mo–S bond distances range from 2.4167(11) to 2.5032(14) Å within the Mo_6S_8 unit and from 2.3908(8) to 2.6262(11) Å within the Mo_9S_{11}. Each $Mo_9S_{11}S_6$ unit is interconnected to 6 $Mo_6S_8S_6$ units (and vice-versa) via

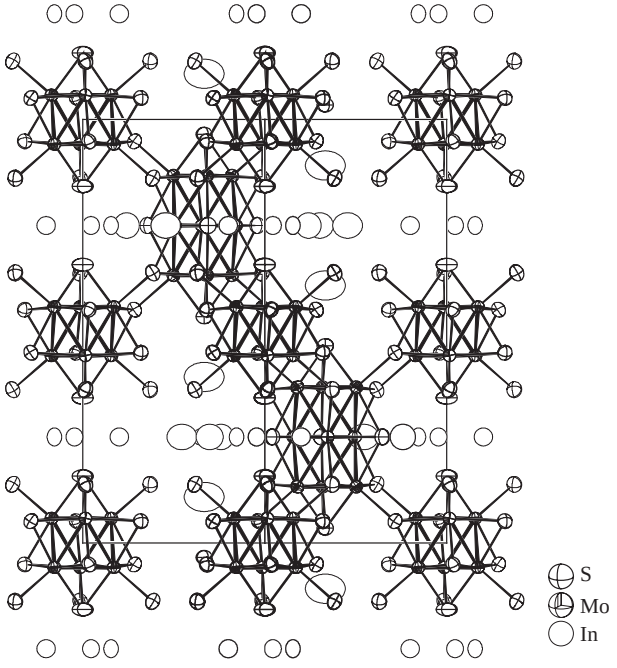

Fig. 1. View of the $In_{3.7}Mo_{15}S_{19}$ structure. Displacement ellipsoids are drawn at the 97% of probability level.

Mo1–S2 bonds (respectively, Mo2–S1) (Fig. 2) to form the three-dimensional Mo–S framework, the connective formula of which is $Mo_9S^i_5S^{i-a}_{6/2}S^{a-i}_{6/2}Mo_6S^i_2S^{i-a}_{6/2}S^{a-i}_{6/2}$. It

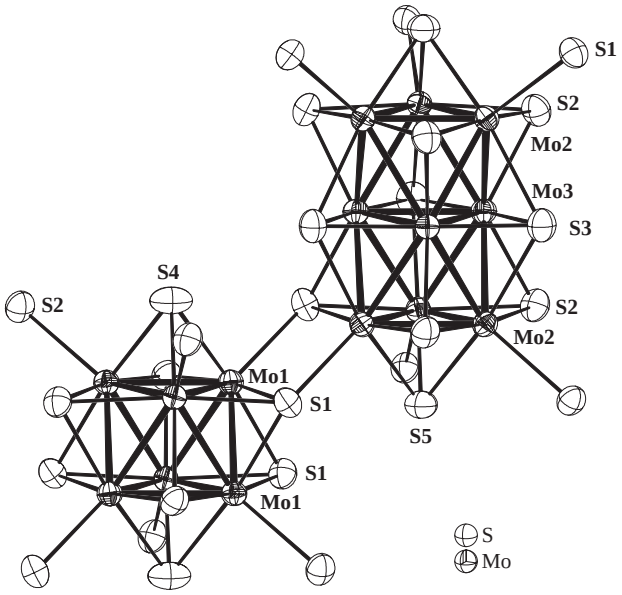

Fig. 2. The $Mo_6S_8S_6$ and $Mo_9S_{11}S_6$ units.

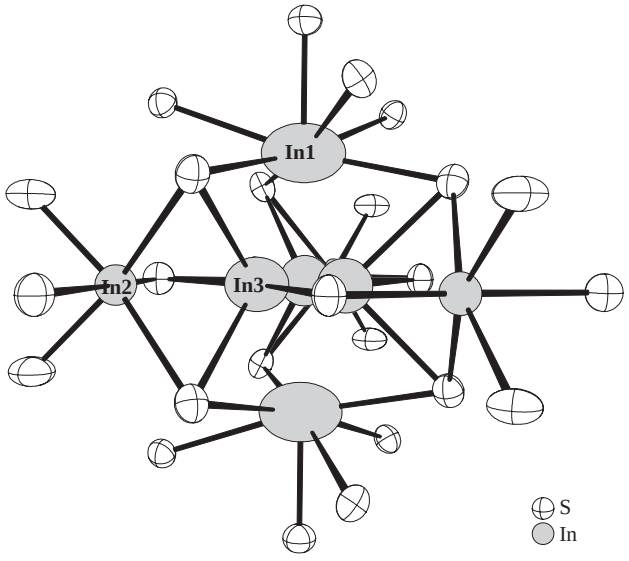

Fig. 3. The three different In sites in $In_{3.7}Mo_{15}S_{19}$.

results from this arrangement that the shortest inter-cluster Mo1–Mo2 distance between the Mo_6 and Mo_9 clusters is in the 3.0780(3)–3.2574(4) Å range in the $In_xMo_{15}S_{19}$ compounds, indicating only weak metal–metal interaction.

3.2. In environments

In $In_{3.7}Mo_{15}S_{19}$, the indium atoms are distributed over three sites (Fig. 3). We find two In atoms at the 4*f* and 6*h* positions as in $In_{3.3}Mo_{15}Se_{19}$ [2]. The first position In1 is fully occupied and corresponds to a large seven-coordinated site of chalcogen atoms. The In1–S distances that range between 2.710(2) and 3.259(1) Å in $In_{3.7}Mo_{15}S_{19}$ suggest clearly that the In1 ion is monovalent. The second position, occupied at 33% corresponds to a triangular group of distorted octahedral sites. The In2–S distances, which range from 2.4570(9) to 2.930(1) Å are much shorter than for the In1 site and, thus reflect the trivalent state of In2. The third site occupied by the In atoms at 23% in $In_{3.7}Mo_{15}S_{19}$ corresponds to a 6*h* position with four In3–S distances in the range 2.871(3)–3.257(3) Å. The latter distances are in agreement with a monovalent indium. Crystal structures made on the $In_xMo_{15}S_{19}$ compounds with $x<3.7$ show that the first indium atoms that are removed are the monovalent In3, then the monovalent In1 and finally the trivalent In2 ions (Fig. 4).

3.3. Evolution of the Mo–Mo bonds in the $In_xMo_{15}S_{19}$ ($0\leqslant x\leqslant 3.7$) series

It is well known that the Mo–Mo distances within the Mo clusters are affected by the cationic charge transfer. So, it was interesting to follow the variations of the Mo–Mo distances within the Mo_6 and Mo_9 clusters of the $In_xMo_{15}S_{19}$ series with respect to the cationic charge.

3.3.1. Mo_6 cluster

In Fig. 5a, we have plotted the Mo–Mo distances within the Mo_6 cluster as a function of the cationic charge. The Mo1–Mo1 intratriangle distances which correspond to the distances within the Mo_3 triangles formed by the Mo atoms related through the three-fold axis vary between 2.6762 and 2.7125 Å and the Mo1–Mo1 between the Mo triangles range from 2.6876 to 2.8507 Å. The most striking feature is the quasi-linear decrease of the intertriangle Mo1–Mo1 distance when the cationic charge increases. This results in a more contracted and regular Mo_6 octahedron in the In-rich compounds while the Mo_6 is elongated along the *c*-axis in the In-poor phases. This behavior is similar to that encountered in the Chevrel phase $Cu_xMo_6S_8$ containing only octahedral Mo_6 clusters for which it was found that the contraction of the Mo_6 octahedron is proportional to the Cu concentration. In particular, the Mo–Mo distances within the Mo_6 cluster in $In_{3.7}Mo_{15}S_{19}$ are close to those observed in $Cu_{3.66}Mo_6S_8$ [10]. This clearly indicates that the formal metal electron count on the Mo_6 cluster should be similar in both compounds, namely 23.66, and thus close to the closed-shell configuration which corresponds to 24 electrons per Mo_6 cluster [11]. On the other, in the In-free compound $Mo_{15}S_{19}$, the Mo–Mo distances within the Mo_6 cluster are similar to those found in the binary Mo_6S_8 [12]. As a consequence, we could estimate the formal electron count on the Mo_6 cluster present in $Mo_{15}S_{19}$ to be close to 20.

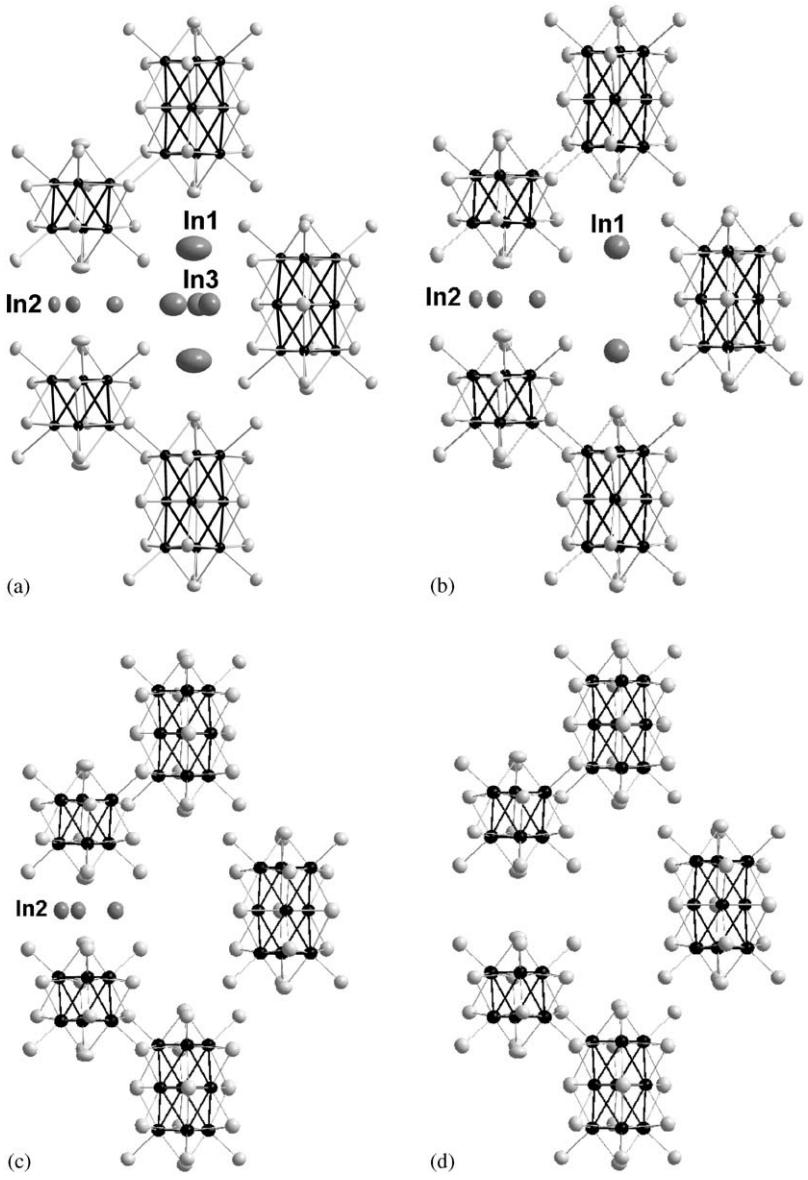

Fig. 4. Views of the In sites showing the hierarchical removal of the In ions: (a) $In_{3.7}Mo_{15}S_{19}$, (b) $In_{2.84}Mo_{15}S_{19}$, (c) $In_{0.7}Mo_{15}S_{19}$, and (d) $Mo_{15}S_{19}$.

3.3.2. *Mo_9 cluster*

Within the Mo_9 cluster (Fig. 5b), if we except the Mo3–Mo3 distances in the median triangle that increase, all the other Mo–Mo distances decrease when the cationic charge increases. The variations of the Mo–Mo distances are smaller than those observed in the Mo_6 cluster since the greatest difference observed for the Mo3–Mo3 bond is of the order of 0.06 Å instead of 0.16 Å in the Mo_6 cluster.

3.4. *Theoretical calculations*

Total and projected DOS, and various COOP curves for different Mo–Mo contacts for the binary compound $Mo_{15}S_{19}$ are sketched in Figs. 6 and 7. Assuming the monovalency of In1 and In3 and the trivalency of In2, one can consider the charge distribution $[In_{3.7}]^{5.7+}[Mo_{15}S_{19}]^{5.7-}$. Therefore the Fermi level for $[Mo_{15}S_{19}]^{6-}$ is also shown. The projection of the frontier molecular orbitals (FMO) of the $Mo_6S_8S_6$ cluster (not displayed here) shows the presence of 20 ME localized on this unit. The peak that lies just above the Fermi level derives in part from the e levels of the molecular orbital (MO) diagram of the Mo_6S_{14} that are empty for 20 ME. As shown by the COOP curves displayed in Fig. 7a, the bands that derive from this orbital are weakly Mo1–Mo1 antibonding within the Mo_3 triangles and Mo1–Mo1 bonding between the triangles. Assuming a rigid band model, a weak lengthening and a shortening of Mo1–Mo1 contacts within the Mo_3 triangles and

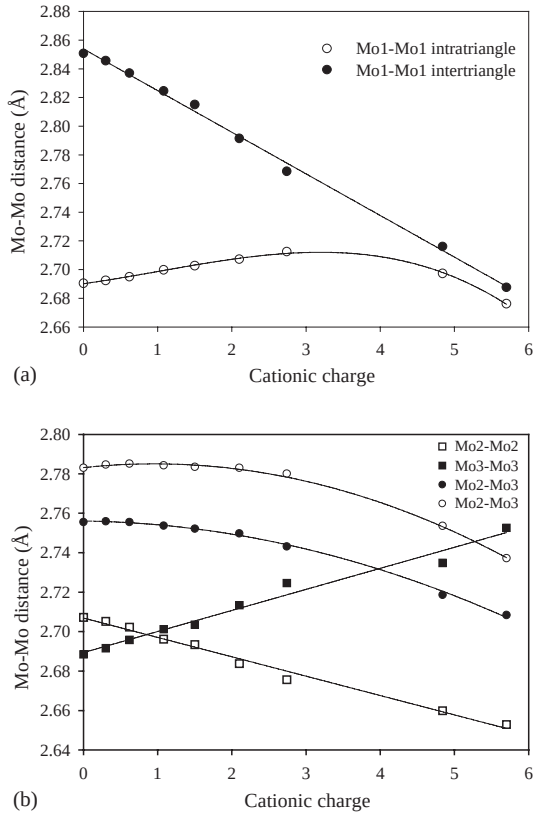

Fig. 5. Variations of the Mo–Mo distances within the Mo_6 (a) and Mo_9 (b) clusters as a function of the cationic charge.

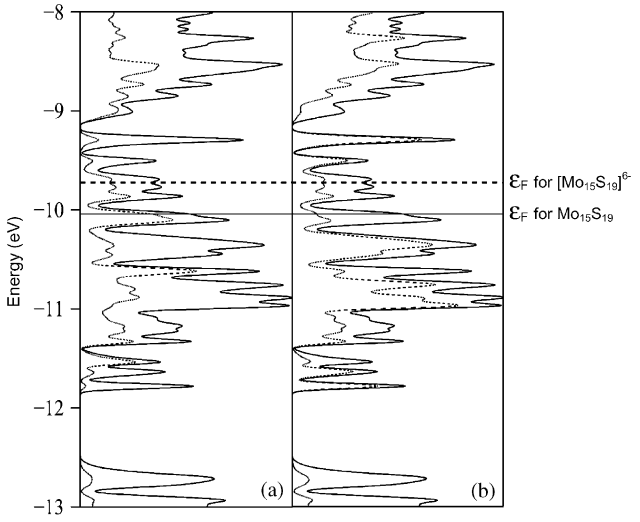

Fig. 6. EHTB calculations for $Mo_{15}S_{19}$ total density of states (plain) and Mo contribution (dotted): (a) Mo_6 and (b) Mo_9.

between the triangles, respectively, is foreseen when the ME count increases. Such an evolution is observed in the crystallographic structure of the $In_xMo_{15}S_{19}$ compounds. Considering the localization of the In ions, an increase of the distances between the Mo_6 and Mo_9

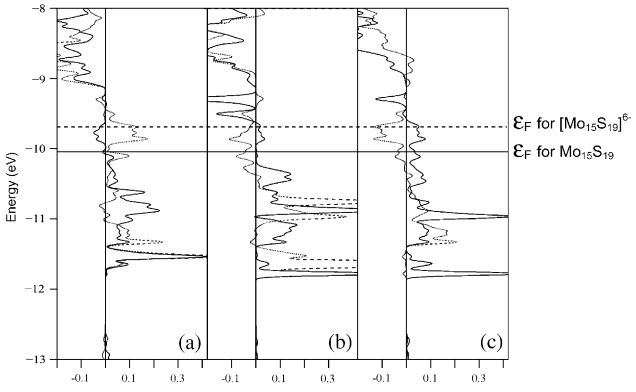

Fig. 7. EHTB calculations for $Mo_{15}S_{19}$: (a) Mo1–Mo1 COOPs for interatomic distances of 2.6899 Å (plain) and 2.8504 Å (dotted), (b) Mo2–Mo2 (plain) and Mo3–Mo3 (dotted) COOPs for interatomic distances of 2.7076 and 2.6900 Å, respectively (c) Mo2–Mo3 (plain) COOP for interatomic distances of 2.7556 and 2.7835 Å, and Mo1–Mo2 (dotted) COOPs for interatomic distances of 3.0780 Å.

clusters is foreseen as a consequence of steric effects. Intercluster COOP curve displayed in Fig. 7c shows that such an evolution is also foreseen because of the Mo1–Mo2 antibonding character of the bands occupied when the ME count of the system increases. Previous theoretical studies have shown that the optimal ME count for the Mo_9 cluster is equal to 36 [11,13,14]. Assuming for the Mo_6 unit a count of 20 in the binary compound $Mo_{15}S_{19}$ and a count closed to 24 ME in $In_{3.7}Mo_{15}S_{19}$, 32 ME are therefore localized on the Mo_9 cluster in $Mo_{15}S_{19}$ and a count closed to 34 ME for the same cluster in $In_{3.7}Mo_{15}S_{19}$. The projection of the frontier molecular orbitals (FMO) of the $Mo_9S_{11}S_6$ cluster (not displayed here) confirm these ME counts. From 32 to 34, the MO diagram of $Mo_9S_{11}S_6$ (see Refs. [11,12]) shows that the extra electrons lie in a MO that presents a Mo3–Mo3 antibonding character and a Mo2–Mo3 and Mo2–Mo2 bonding character. Similar properties are shown by the bands that lie just above the Fermi level and that will be occupied if the ME count increases (Fig. 7). The lengthening of the Mo3–Mo3 contacts and the shortening of the Mo2–Mo2 and Mo2–Mo3 distances that can be envisioned theoretically when extra electrons are added, is observed experimentally in the crystallographic structure of the $In_xMo_{15}S_{19}$ compounds when x increases. Because its optimal ME count of 36 is not reached in $In_{3.7}Mo_{15}S_{19}$, it should be possible to add more electrons on the Mo_9 cluster.

3.5. Magnetic susceptibility measurements

The magnetic susceptibility measurements were carried out on batches of single crystals of about 100 mg in an applied field of 20 Oe using a DC SQUID magnetometer. All samples investigated ($x = 0.0$, 0.5, 2.84 and 3.7) show a diamagnetic shielding signal below 4 K

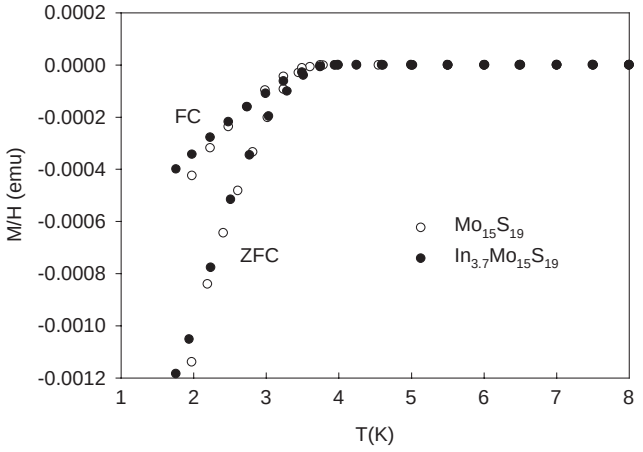

Fig. 8. Temperature dependence of the magnetic susceptibility for $In_{3.7}Mo_{15}S_{19}$, and $Mo_{15}S_{19}$. The magnetic field applied was 20 Oe for zero-field-cooling (ZFC) and field-cooling (FC) modes.

indicating a superconducting transition as illustrated in Fig. 8 for the two ending members $In_{3.7}Mo_{15}S_{19}$ and $Mo_{15}S_{19}$. This metallic behavior is in agreement with the theoretical calculations. Finally, it should be mentioned that Tarascon et al. [3] did not observed superconductivity in the $In_xMo_{15}S_{19}$ ($x<3.4$) compounds prepared under HCl gas at temperature ranging between 370°C and 550°C.

A further step in this study would be to replace partially or totally the monovalent indium by another monovalent cation such as rubidium, cesium or thallium and the trivalent indium by a trivalent rare earth, for example. On the other hand, works are in progress to follow the evolution of the crystal structure of the binary $Mo_{15}S_{19}$ as a function of the temperature by X-ray single-crystal diffraction.

Supporting information available

Further details of the crystal structure investigations can be obtained from the Fachinformationszentrum Karlsruhe, 76344 Eggenstein-Leopoldshafen, Germany (fax: (49) 7247-808-666; e-mail: crysdata@fiz.karlsruhe.de), on quoting the depository number CSD-413399, CSD-413400, CSD-413401, CSD-413402, CSD-413403, CSD-413404, CSD-413405, and CSD-413406.

Acknowledgments

Intensity data were collected on the Nonius Kappa CCD X-ray diffactometer system of the 'Centre de diffractométrie de l'Université de Rennes I' (www.cdifx.univ-rennes1.fr).

References

[1] D. Salloum, P. Gougeon, M. Potel, J. Alloys Compounds, 2004, in press.
[2] A. Gruttner, K. Yvon, R. Chevrel, M. Potel, M. Sergent, B. Seeber, Acta Crystallogr. B 35 (1979) 285.
[3] J.M. Tarascon, G.W. Hull, Mater. Res. Bull. 21 (1986) 859.
[4] B.V. Nonius, COLLECT, data collection software, Nonius BV, 1999.
[5] A.J.M. Duisenberg, Reflections on Area Detectors, Ph.D. Thesis, Utrecht, 1998.
[6] J. de Meulenaar, H. Tompa, Acta Crystallogr. A 19 (1965) 1014–1018.
[7] V. Petricek, M. Dusek, Jana2000, Institute of Physics, Academy of Sciences of the Czech Republic, 2000.
[8] (a) R. Hoffmann, J. Chem. Phys. 39 (1963) 1397.
(b) M.-H. Whangbo, R. Hoffmann, J. Am. Chem. Soc. 100 (1978) 6093.
[9] G.A. Landrum, YAeHMOP, Yet Another extended Hückel Molecular Orbital Package, Ithaca, NY, 1997 (release 2.0).
[10] K. Yvon, A. Paoli, R. Flükiger, R. Chevrel, Acta Crystallogr. B 33 (1977) 3066.
[11] T. Hughbanks, R. Hoffmann, J. Am. Chem. Soc. 105 (1983) 1150.
[12] R. Chevrel, M. Sergent, J. Prigent, Mater. Res. Bull. 9 (1974) 1487.
[13] R. Gautier, P. Gougeon, J.-F. Halet, M. Potel, J.-Y. Saillard, J. Alloys Compounds 262–263 (1997) 311.
[14] S. Picard, J.-F. Halet, P. Gougeon, M. Potel, Inorg. Chem. 38 (1999) 4422.